The evolution of the Eastern Himalayan syntaxis revealed by India (Tethyan Himalaya Series) in central Myanmar

Myo Min[1,2], Lothar Ratschbacher[1], Leander Franz[3], Bradley R. Hacker[4], Eva Enkelmann[5], Eko Yoan Toreno[1], Raymond Jonckheere[1], Birk Härtel[1], Bernd Schurr[6], Marion Tichomirowa[1], Jörg A. Pfänder

[1]Geowissenschaften, TU Bergakademie Freiberg, Freiberg, Germany, [2]Geology Department, University of Mandalay, Mandalay, Myanmar, [3]Mineralogisch-Petrologisches Institut, Universität Basel, Basel, Switzerland, [4]Geological Sciences, University of California, Santa Barbara, USA, [5]Department of Geosciences, University of Calgary, Alberta, Canada, [6]German Research Center for Geoscience, Potsdam, Germany

Corresponding author: Lothar Ratschbacher (lothar@geo.tu-freiberg.de)

Key Points:

- Indian-affinity Tethyan Himalaya Series occur in central Myanmar, ~450 km south of the Himalayan rocks in the Eastern Himalayan Syntaxis
- A low temperature-high pressure subduction-early collision setting was active at ~65 Ma, peaked at ~45 Ma, and ended at ~30 Ma
- The Sagaing transform fault reactivated the Indus-Yarlung suture, and imbricated the Indian rocks and the Burma microplate from ~30 Ma on

Abstract

In the Katha Range of central Myanmar, lithologic tracers and pressure-temperature-deformation-time data identify Cambro-Ordovician, Indian-affinity Tethyan Himalaya Series (THS), located ~700 km from their easternmost outcrop in S-Tibet and ~450 km from Himalayan rocks in the Eastern Himalayan Syntaxis (EHS). Metamorphism began at ~65 Ma, peaked at ~45 Ma (~510°C, 0.93 GPa), and exhumation/cooling (~25°C/Myr) occurred until ~30 Ma in a subduction-early collision setting. When the Burma microplate—part of the intra-Tethyan Incertus-arc—accreted to SE-Asia, its eastern boundary, the southern continuation of the Indus-Yarlung suture (IYS), was reactivated as the Sagaing fault (SF), which propagated northward into Indian rocks. In the Katha rocks, this strike-slip stage is marked by ~4°C/Myr exhumation/cooling. Restoring the SF system defines a continental collision-oceanic subduction transition junction, where the IYS bifurcates into the SF at the eastern edge of the Burma microplate and the Jurassic ophiolite-Jadeite belt that includes the Incertus suture.

Plain Language Summary

Central Myanmar hosts rocks typical for the northernmost continental crust of the Indian continent. These rocks are now located ~700 km from their easternmost outcrop in S-Tibet and ~450 km from Himalayan rocks in the Eastern Himalayan Syntaxis—the eastern edge of India. They record an oceanic subduction-early collision setting from ~65 to 30 Ma. Our findings aid to the restauration of the Sagaing transform-fault (SF) system at the eastern edge of India. The SF system imbricated the Indian-affinity rocks, and the Burma microplate—part of the intra-Tethyan Incertus-arc.

1. Introduction

Indenter corners in collisional orogens—syntaxes—feature 3-D deformation with crustal thickening, lateral material flow, and transitions from continental to oceanic subduction. In the Cenozoic India-Asia collision zone, the underthrusting Indian craton has induced shortening in the Himalaya and Tibet, and lateral material flow out of the collision zone (e.g., Zhang et al., 2004; Zubovich et al., 2010). Pronounced lateral flow and clockwise vertical-axis rotations occur at the Eastern Himalayan Syntaxis (EHS) where the Himalayan continental subduction transitions into the highly-oblique Burma oceanic subduction zone and the Sagaing transform-fault (SF) system (Figure 1a). Paleomagnetic studies in the Burma microplate, and the Asian-affinity Tengchong (Lhasa) and Baoshan (Qiangtang-Sibumasu) blocks indicate 40–90° clockwise, vertical-axis rotations in Myanmar and Yunnan since the Paleocene, changing the original ~W-strike of these blocks in Tibet to a ~N-strike south of the EHS (e.g., Kornfeld et al., 2014; Li et al., 2018, 2020; Westerweel et al., 2019).

Northward-widening cratonic India extends northeastward into the EHS region, and is rimmed in the east by the oceanic lithosphere of the Bay of Bengal. The current transition from continental collision to oceanic subduction must occur in the Indo-Burman Ranges (IBR), part of the Jurassic-Recent subduction-accretionary wedge that bounds the Indian plate in the east, because the footwall of the northern IBR is made up of the Indian continental crust of the Shillong Plateau (Figure 1a). The past position of this transition is unclear due to the intervening Burma microplate and the northward-growing SF system, disrupting the Burma microplate, the IBR wedge, and the southern prolongation of the Indus-Yarlung suture (IYS) between India and Asia (e.g., Baxter et al., 2011).

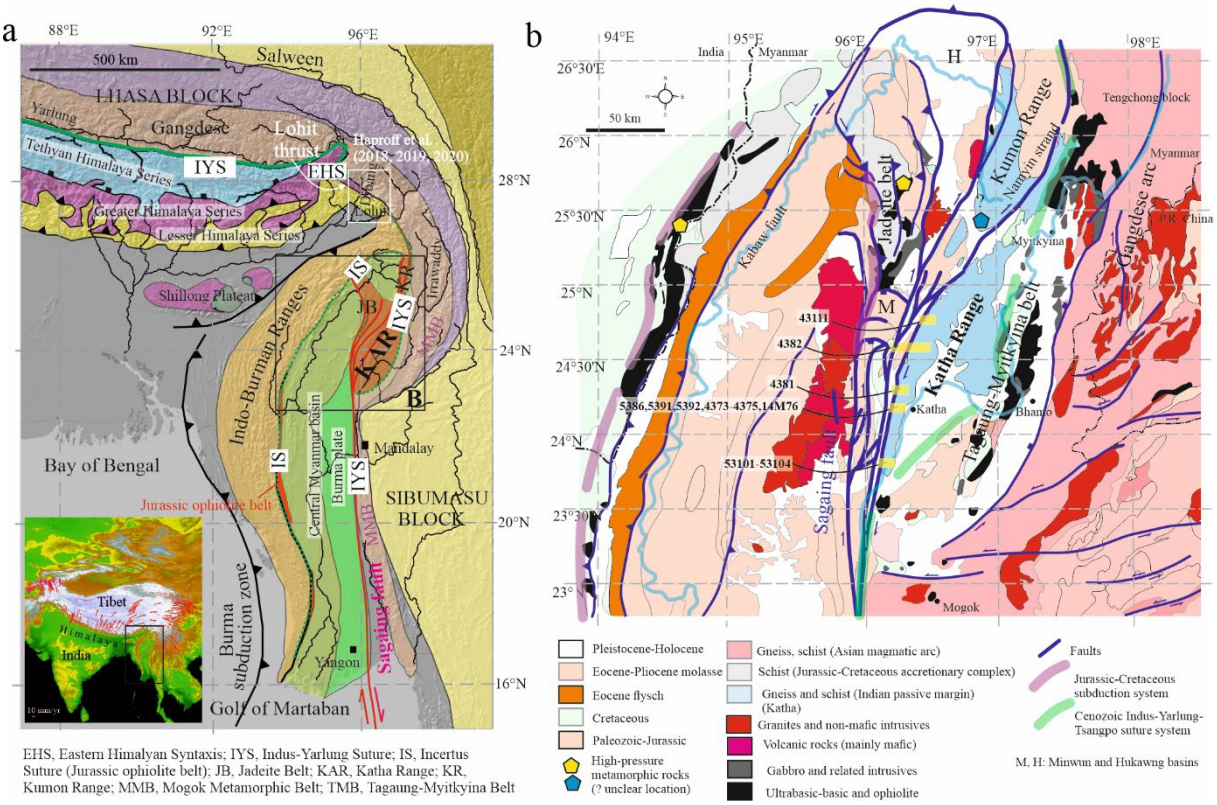

EHS, Eastern Himalayan Syntaxis; IYS, Indus-Yarlung Suture; IS, Incertus Suture (Jurassic ophiolite belt); JB, Jadeite Belt; KAR, Katha Range; KR, Kumon Range; MMB, Mogok Metamorphic Belt; TMB, Tagaung-Myitkyina Belt

Figure 1. a) Eastern Himalayan Syntaxis and eastern margin of the Indian plate (modified from Robinson et al., 2014). Insert locates a) and shows Eurasia-fixed GNSS-derived displacement field. b) Geological map centered on the Katha Range modified from Geological Map of Myanmar (2014) and Wang & Burchfiel (1997). Sagaing transform-fault system modified from Morley & Arboit (2019) and Maurin et al. (2010). Yellow bars: studied traverses and samples.

To account for the ≥50 Ma onset of the India-Asia collision (e.g., Hu et al., 2016), a northern extension of cratonic India has been proposed. This Greater India is envisioned as a <2000-km-wide northward-projecting entity, consisting of extended continental and oceanic Indian lithosphere (e.g., van Hinsbergen et al., 2012) that has along its northern rim the Tethyan Himalaya Series (THS), on which the ophiolites of the IYS were emplaced.

Given that India's northward motion has been accommodated by subduction/shortening of Greater Indian and cratonic Indian lithosphere, lateral material flow out of the collision

zone, and northward propagation of the Burma subduction zone and the SF system, tracing the evolution of the continental collision-oceanic subduction transition, describing the initiation and evolution of the SF system, and reconstructing the eastern edge of Greater India are key aspects of understanding the India-Asia collision zone and of indenter corners in general. Here, we trace the eastern edge of India—represented by the THS—into central Myanmar. In the Katha Range, lithologic tracers and pressure-temperature-deformation-time (P-T-d-t) data outline a piece of the basal Cambro-Ordovician THS that experienced high-P–low T metamorphism, exhumed rapidly in a subduction-early collisional setting, and was involved into the northward growth of the SF system. The Katha rocks allow the timing of the activity in the subduction-early collisional setting and of the onset of strike-slip faulting along the SF system, and aid in the restauration of the eastern margin of India.

2. The eastern Himalayan Syntaxis Region

Haproff et al. (2018, 2019, 2020) and Salvi et al. (2019) mapped the lithologic units of India and Asia at the EHS (Dibang and Lohit valleys; Figure 1a), encountering the Gangdese arc (Asia), the IYS (Tidding-Mayoda mélange), and the Lesser Himalaya Series (LHS; India, Mayodia gneiss, Lalpani schist). The Greater Himalaya Series (GHS), THS, and Xigaze forearc basin (Asia) are absent.

The NNE-trending Katha Range (Figure 1b) is bounded in the east by the 177–163 Ma (U-Pb zircon) Tagaung-Myitkyina suprasubduction-zone (ultra-)mafic rocks (Yang et al., 2012; Liu et al., 2016), which are intruded by Gangdese-arc granitoids (Zhang et al., 2018). In the west, the Range is bounded by the Namyin strand of the SF system; rocks involved

in its western strands include the Jurassic (Qiu et al., 2009; Shi et al., 2008) Jadeite belt (Figure 1b). Sericite-chlorite-biotite-garnet schist, locally with amphibole, talc, and kyanite, quartzite, and marble have been reported from the Katha Range; their stratigraphic age may cover the early Paleozoic to Triassic (e.g., Mitchell, 2018; Zhang et al., 2018).

3. Katha Range: Lithology, Pressure-temperature-deformation-time Evolution

Lithologically, we encountered porphyroblastic chloritoid-garnet-graphite micaschist, chlorite-chloritoid-bearing white-mica quartzite, and porphyroblastic staurolite-kyanite-garnet quartz micaschist. Locally, the Katha schists and quartzites enclose m-thick meta-acidite tectonites, dominated by phengite and porphyric quartz, interpreted as volcanic layers or small hypabyssal intrusions. We used zircon and rutile U-Pb geochronology to determine igneous emplacement ages, the maximum deposition age of the meta-sedimentary rocks, and to establish correlations with rocks of the Himalaya and S-Tibet. Supporting information Text S1 provides the sample petrography, Text S2 outlines the geo-thermochronologic methods, and Tables S1 to S3 list their results and analytical data.

Two meta-acidites yielded U-Pb zircon crystallization ages of 501 ± 9 and 530 ± 5 Ma (2s; Figure S1 in Supporting Information), both with major inheritance. Figure 2a compares the inherited (meta-acidites) and detrital (meta-sedimentary rocks) U-Pb zircon and rutile ages: the zircon age distributions of all samples are consimilar, with clusters at ~500 and 1000 Ma; nearly all detrital rutile ages are at ~500 Ma. The youngest detrital zircon and rutile grains are 482 +7/-19 and 463 +8/-10 Ma, respectively, calculated with

the "Youngest Zircon" routine and "3rd degree of youngest option" (Isoplot4.5; Ludwig, 2008). These dates suggest a Cambro-Ordovician age for the studied Katha rocks.

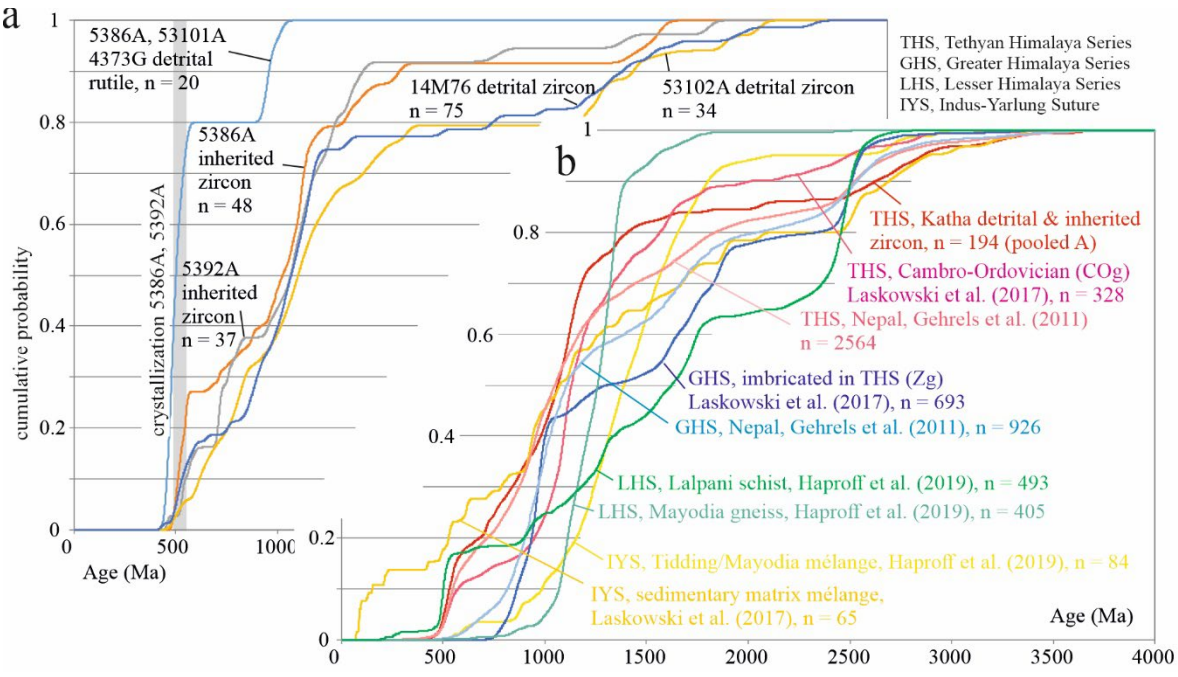

Figure 2. Cumulative probability plots of U-Pb zircon and rutile ages of a) samples from this study and sample 14M76 of Zhang et al. (2018), and b) their comparison with rocks from the central and eastern Himalaya. Ages used include 2s uncertainties and have 90–110% $^{206}Pb/^{238}U$–$^{207}Pb/^{206}Pb$ age concordance.

Figure 3a plots the Katha-rock P-T data together with THS data from central S-Tibet (Laskowski et al., 2016), eastern S-Tibet (Dunkl et al., 2011, Fang et al., 2020), and GHS and LHS data from Bhutan (Daniel et al., 2003). Table S4 of the Supporting Information summarizes our P-T results, and Text S1 details the petrology, derived from THERIAK/DOMINO equilibrium-assemblage calculations and conventional thermobarometry. Four meta-sedimentary rocks yielded prograde P-T data of 470–510°C, 1.0–1.5 GPa and peak data at 490–551°C, 0.8–1.0 GPa; one sample has higher temperatures (prograde ~535°C, 1.0 GPa, peak ~650°C, 1.0 GPa). Figure 3b plots the Katha-rock T-t history. The meta-acidite zircon ages, the youngest detrital zircon age groups, and the detrital rutile ages (all U-Pb) indicate a Cambro-Ordovician intrusion

(zircon) and cooling (rutile) event. U-Pb monazite and rutile, Rb-Sr phengite, $^{40}Ar/^{39}Ar$ phengite and biotite, zircon (ZFT) and apatite fission track (AFT), and zircon (U-Th)/He (ZHe) dates outline the Cenozoic evolution. We calculated closure-temperatures, T_c, with CLOSURE (Brandon et al., 1998). For Ar/Ar phengite, we used a T_c of ~450°C, accounting for slower diffusional loss at elevated pressures (e.g., Harrison et al., 2009; Warren et al., 2012). Changes in the actual T_c have little effect on the first-order T-t history.

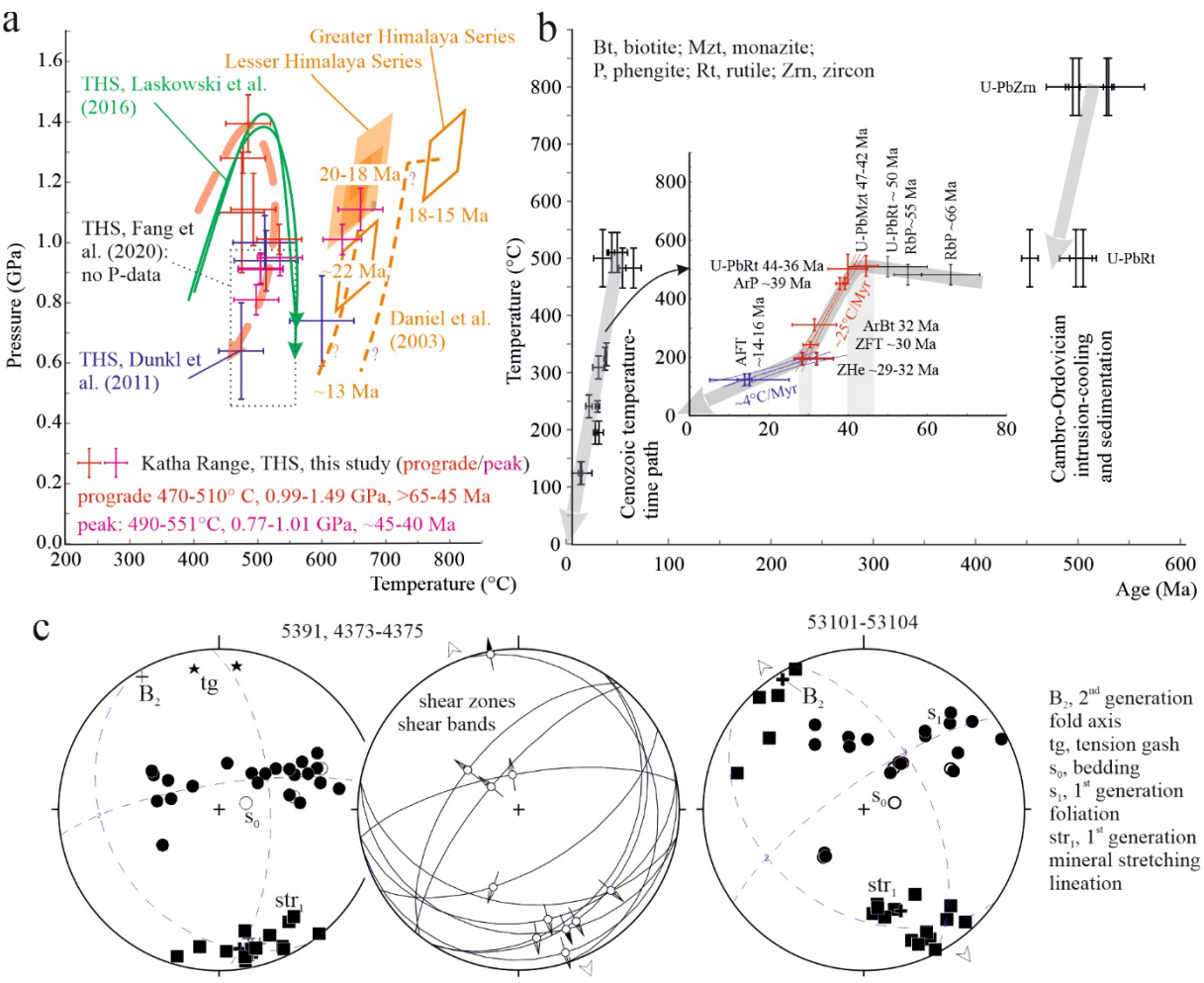

Figure 3. Pressure-temperature-time-deformation (P-T-t-d) data. a) P-T of the Katha rocks and comparison with data from central and eastern S-Tibet and the eastern Himalaya. b) T-t paths, and c) structural data of the Katha rocks; see Figure 1b for traverses studied.

Given a ~550°C T_c for the Rb-Sr phengite system (e.g., Blanckenburg et al., 1989)—higher than the average peak-T (~510°C)—the two dates ≥55 Ma likely are formation ages during prograde metamorphism (~483°C average T). The same may apply for the U-Pb rutile date (~50 Ma; T_c of 500–650°C; e.g., Kooijman et al., 2010; Ewing et al., 2015) of quartzite 53101A, whose 500–800°C T-range from Zr-in-rutile isopleths (Figure S1 of Supporting Information) indicates incomplete reset of detrital rutile. The 500–550°C Zr-in-rutile-derived T-range of 44–36 Ma rutiles indicates metamorphic growth in meta-acidite 5386A, different from the higher-T of inherited grains (Figure S1 of Supporting Information). Peak-T is likely best dated by the 48–42 Ma monazite inclusions (~10 μm) in poikiloblastic kyanite of sample 4382. Taken together, the T-t path comprises prograde metamorphism from ~65 Ma to peak P-T at ~45 Ma (~55 km burial, assuming a lithostatic gradient of ~37 km/GPa), cooling at ~25°C/Myr to ~30 Ma, and cooling at ~4°C/Myr thereafter (Figure 3b).

Figure 3c compiles structural data of the Katha rocks along two traverses. Bedding (s_0) and foliation (s_1) occupy a great-circle distribution, recording open to tight folds with ~NNW-trending axes (B_2), subparallel to mineral stretching lineation str_1. S_1 and str_1 are associated with folded shear zones/bands that indicate ~NNW-SSE stretch with dominant top-to-SSE shear, also indicated by σ-clasts and asymmetric foliation boudinage. Overprinting a relict fabric, s_1, str_1, and the shear fabrics are outlined by the syn- to post-peak P-T mineral assemblage; they likely record exhumation by crustal extension. The folds record the regional ~E-W shortening south of the EHS (e.g., Wang & Burchfiel, 1997).

3. Discussion

We focus on four salient questions: What Himalaya-Tibet series do the Katha rocks represent? How and when were they exhumed? Which position did they occupy in the evolution of the India-Asia collision system? When and how were they involved in the oblique plate boundary south of the EHS?

Lithologically, the Katha rocks are part of the THS and most similar to the Cambro-Ordovician gneiss-schist unit in central S-Tibet (Laskowski et al., 2017). Figure 2b compares the inherited and detrital zircon ages of the Katha rocks with equivalents, i.e., the Cambro-Ordovician THS of central S-Tibet, the Nepal THS, the central Himalaya and Nepal GHS, the LHS units at the EHS, the IYS in the central Himalaya and at the EHS (Gehrels et al., 2011; Laskowski et al., 2016; Haproff et al., 2019); we chose these units because of their proximity to the EHS, P-T-t-d history (central Himalaya), and large database (Nepal). The Katha rocks compare best to the THS, and least to the IYS, LHS, and GHS rocks.

Petrologically, the Katha-rock data (Figure 3a; red P-T path) are most similar to the THS data of central S-Tibet (Figure 3a; green P-T paths; Laskowski et al., 2016); there, metamorphism at ≥1.4 GPa, ≤600°C peaked at ~40 Ma and the rocks cooled rapidly through 39–34 Ma. The basal THS rocks of eastern S-Tibet experienced comparable-T but lower-P (~600°C, 0.78 GPa; Dunkl et al., 2011; 510 ± 50°C, Fang et al., 2020; Figure 3a) and burial-early exhumation histories like those inferred for Katha (~49–32 Ma; U-Pb zircon, K(Ar)/Ar mica; e.g., Ratschbacher et al., 1994; Aikman et al., 2008, 2012; Dunkl et al., 2011). Post-thrusting uppermost GHS granitoids in the same area have 48–36 Ma U-Pb zircon ages; the associated schists show higher-T and lower-P (~630–660°C, 0.7–0.8 GPa; Ding et al., 2016a, b) than the Katha rocks. Different from the latter, both the THS and GHS rocks experienced Miocene rapid cooling (~18–12 Ma; e.g., Aikman et al., 2008, 2012;

Dunkl et al., 2011; Ding et al., 2016a). The IYS rocks of the southern EHS (Tidding-Mayodia mélange) record metamorphism and ~30°C/Myr cooling between 40–30 Ma and rapid Miocene cooling (~11–6 Ma; ZHe ages; Haproff et al., 2020), not documented in the Katha rocks. The Katha P-T-t data contrast with GHS and LHS data in Bhutan (Figure 3a; e.g., Daniel et al., 2003). Lithology and P-T-t evolution are compatible with the Katha rocks being a piece of the basal—Cambro-Ordovician—THS, now located ~700 km of the THS in eastern S-Tibet and ~450 km south of the Himalayan rocks in the Lohit valley at the southern edge of the EHS.

Structural studies in eastern S-Tibet outlined top-to-S thrusts and S-facing folds, overprinted by N-facing folds close to the Great Counter Thrust along the IYS (e.g., Ratschbacher et al., 1994; Dunkl et al., 2011). Detachments—most with top-to-N kinematics—separate the GHS and THS and occur within the basal THS (e.g., Ding et al., 2016a,b). In the southern EHS, Haproff et al. (2018) mapped thrusts with a ≤90° clockwise change in displacement directions. The Katha rocks preserve—besides relict deformation—fabrics akin to the normal-sense detachments in the THS. Assuming 60–90° clockwise rotation due to the motion of the Himalayan (THS of Katha) and Asian (Tengchong–Gangdese) rocks of central and eastern Myanmar and Yunnan around the EHS, the top-to-SSE flow in the Katha THS rocks restores to top-to-~E flow, deflected ~90° from the typical top-to-N flow in S-Tibet. The younger, ~NNW-trending folds parallel the present-day structural grain and appear unrotated.

Whereas the exhumation history is comparable to other THS localities, two aspects of the Katha rocks stand out: the lack of a Miocene cooling event and the top-to-~E normal-sense exhumation. We attribute the ~45–30 Ma rapid cooling as due to exhumation from ~55-

km-depth in a subduction-early collision setting at the leading edge of Greater India, as observed in other THS rocks. The top-to-~E exhumation kinematics may indicate that the Katha rocks were positioned at the easternmost end of the Himalaya.

The initiation of the SF system has been bracketed to middle Miocene-early Pliocene, based on the onset of seafloor spreading in the Andaman rift (e.g., Bertrand & Rangin, 2003). Morley & Arboit (2019) proposed a 28–27 Ma onset, based on the age of the basal strata in a releasing-bend basin (Minwun basin, Figure 1b) along a SF strand in northern Myanmar. The change from ~25 to ~4°C/Myr cooling of the Katha rocks at ~30 Ma may signify their involvement into the SF system, when it started to interact with the THS thrust-fold belt that acquired a ~N-strike during the northward propagation of India's eastern tip. The movement around the EHS also allowed the Katha rocks to escape the intense shortening at the collision front, thus a Miocene overprint.

Figure 4 summarizes our proposed evolution of the EHS and the SF system: At ~60 Ma (Figure 4a), the Incertus-arc system—which the Burma microplate was part of—terminated (Westerweel et al., 2019). The highly-oblique plate boundary along Greater India's eastern margin offset the Burma microplate (at ~5°N) from the leading Greater India subduction in the north; collision with the Indian margin rotated it ~40° clockwise (~60–40 Ma; Li et al., 2020). Continental subduction may have started at ≥47 Ma at both syntaxes, as indicated in the western Himalaya (Tso Morari; Donaldson et al., 2013) and the Katha range. The IYS at the eastern edge of the Burma microplate was reactivated as the SF system (Figure 4b); its ~30 Ma initiation terminated the Katha-rock exhumation in the subduction-collision setting and the transition to strike-slip motion with little exhumation. The SF system connected with the THS thrust-fold belt at the EHS, where the

THS were later subducted together with the GHS (Haproff et al., 2020). Figures 4c and 4d show the evolution of the SF system: the eastern Namyin strand allows restoration of the Jadeite belt to the south, at least to the southern tip of the Indian rocks—south of the Katha Range; a western strand and the Kabaw fault allows restoration of the Jurassic ophiolite belt, connecting it to the south of the Jadeite belt. The entire area south of the EHS—including the SF system—experienced clockwise rotation and ~E-W shortening during the evolution of the Burma subduction system and the collision of the northward-moving Burma microplate with the Shillong plateau.

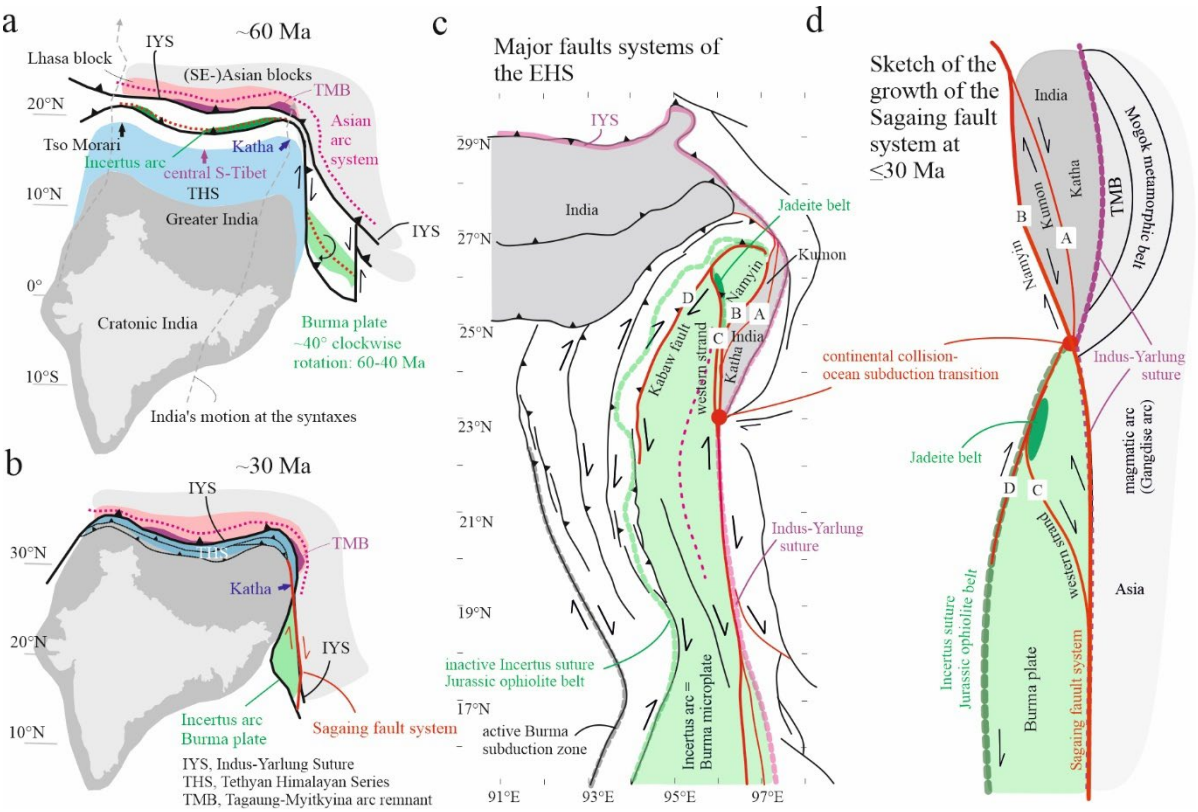

Figure 4. The Katha Range in the evolution of the Eastern Himalayan Syntaxis (EHS) and the Sagaing fault system (SF). a) Incipient Himalaya formation following Incertus-arc subduction with the Burma microplate at the arc's eastern end. b) Development of the SF system along the Indus-Yarlung suture (IYS) and its connection with the Tethyan-Himalaya fold-thrust belt. c) Major fault systems of the EHS. d) Restoration of the imbrication of the Incertus-arc subduction system at the western margin of the Burma microplate.

Growth of the SF system isolated the Jadeite belts and imbricated the Indian rocks of the Katha and Kumon Ranges.

Acknowledgments

Funded by DFG RA 442/28.

Conflict of Interest

The authors declare no conflicts of interest relevant to this study.

Open Research

The petrologic and geo-thermochronologic data are available as Supporting Information in the online version of this article and (CC-BY 4.0 license) on the OpARA server of TU Bergakademie Freiberg and TU Dresden at http://dx.doi.org/10.25532/OPARA-xxx (will be open when excepted).

References

Aikman, A.B., Harrison, T.M., & Ding, L. (2008). Evidence for early (>44 Ma) crustal thickening, Tethyan Himalaya, southeastern Tibet. *Earth and Planetary Science Letters, 274*, 14–23.

Aikman, A.B., Harrison, T.M., & Hermann, J. (2012). Age and thermal history of Eo- and Neohimalayan granitoids, eastern Himalaya. *Journal of Asian Earth Sciences, 51*, 85–97.

Baxter, A.T., Aitchison, J.C., Zyabrev, S.V., & Ali, J.R. (2011). Upper Jurassic radiolarites from the Naga ophiolite, Nagaland, northeast India. *Gondwana Research, 20*, 638–644.

310 Bertrand, G., & Rangin, C. (2003). Tectonics of the western margin of the Shan Plateau
311 (central Myanmar): Implication for the India-Indochina oblique convergence since
312 the Oligocene. *Journal of Asian Earth Sciences, 21*, 1139–1157.
313 Blanckenburg, v. F., Villa, I.M., Baur, H., Morteani, G., & Steiger, R.H. (1989). Time
314 calibration of a PT-path from the Western Tauern Window, Eastern Alps: the
315 problem of closure temperatures. *Contributions Mineralogy Petrology, 101*, 1-11.
316 Bohlen, S.R., & Liotta J.J. (1986). A barometer for garnet amphiboles and garnet granulites.
317 *Journal of Petrology, 27*, 1025–1034.
318 Brandon, M.T., Roden-Tice, M.K., & Garver, J. I. (1998). Late Cenozoic exhumation of the
319 Cascadia accretionary wedge in the Olympic Mountains, northwest Washington
320 State. *Geological Society of America Bulletin, 110*, 985–1009.
321 Daniel, C.G., Hollister, L.S., Parrish, R.R., & Grujic, D. (2003). Exhumation of the Main
322 Central Thrust from lower crustal depths, eastern Bhutan Himalaya. *Journal*
323 *metamorphic Geology, 21*, 317–334.
324 De Capitani, C. (1994). Gleichgewichts-Phasendiagramme: Theorie und Software. *European*
325 *Journal of Mineralogy, Bh.1, 6*, 48.
326 Ding, H., Zhang, Z., Hu, K., Dong, X., Xiang, H., & Mu, H. (2016a). P-T-t-D paths of the North
327 Himalayan metamorphic rocks: Implications for the Himalayan orogeny.
328 *Tectonophysics, 683*, 393–404.
329 Ding, H., Zhang, Z., Dong, X., Tan, Z., Xiang, H., Mu, H., Gou, Z., Shui, X., Li, W., & Mao, L.
330 (2016b). Early Eocene (*c*. 50Ma) collision of the Indian and Asian continents:
331 Constraints from the North Himalayan metamorphic rocks, southeastern Tibet.
332 *Earth and Planetary Science Letters, 435*, 64–73.

Donaldson, D.G., Webb, A.A.G., Menold, C.A., Kylander-Clark, A.R.C., & Hacker, B.R., (2013). Petrochronology of Himalayan ultrahigh-pressure eclogite. *Geology, 41*, 835–838.

Dunkl, I., Antolín, B., Wemmer, K., Rantitsch, G., Kienast, M., Montomoli, C., Din, L., Carosi, R., Appel, E., El Bay, R., Xu, Q., & von Eynatten, H. (2011). Metamorphic evolution of the Tethyan Himalayan flysch in SE Tibet. *Geological Society, Special Publications, 353*, 45–69.

Ewing, T.A., Rubatto, D., Beltrando, M., & Hermann, J. (2015). Constraints on the thermal evolution of the Adriatic margin during Jurassic continental break-up: U–Pb dating of rutile from the Ivrea–Verbano Zone, Italy. *Contribution Mineralogy Petrology, 169*, doi.org/10.1007/s00410-015-1135-6, 2015

Fang, D-R., Zhang, J., Hisada, K-I., Wang, G-H., & Li D. (2020). Geological anatomy of the Upper Triassic sequence in southeastern Tibet: Implications for tectonic evolution of the eastern Himalayan orogen. *Geological Journal, 55*, 6607–6624.

Farley, K. A., Wolf, R. A., & Silver, L. T. (1996). The effects of long alpha-stopping distances on (U-Th)/He dates. *Geochimica et Cosmochimica Acta, 60*, 4223–4230.

Frei, D., & Gerdes A. (2009). Precise and accurate in situ U-Pb dating of zircon with high sample throughput by automated LA-SF-ICP-MS. *Chemical Geology, 261*, 261–270.

Gehrels, G., Kapp, P., DeCelles, P., Pullen, A., Blakey, R., Weislogel, A., Ding, L., Guynn, J., Martin, A., McQuarrie, N., & Yin, A. (2011). Detrital zircon geochronology of pre-Tertiary strata in the Tibetan-Himalayan orogen. *Tectonics, 30*, https://doi.org/10.1029/2011TC002868

Ghent, E.D., Stout, M.Z., Black, P.M., & Brothers, R.N. (1987). Chloritoid bearing rocks with blueschists and eclogites, northern New Caledonia. *Journal Metamorphic Geology, 5*, 239–254.

Geological Map of Myanmar (2014). 1:2,250,000, Myanmar Geosciences Society.

Haproff, P.J., Zuza, A.V., & Yin, A. (2018). West-directed thrusting south of the eastern Himalayan syntaxis indicates clockwise crustal flow at the indenter corner during the India-Asia collision. *Tectonophysics, 722*, 277–285.

Haproff, P.J., Zuza, A.V., Yin, A., Harrison, T.M., Manning, C M., Ding, L., et al. (2019). Geologic framework of the northern Indo-Burma Ranges: Lateral correlation of Himalayan-Tibetan lithologic units across the eastern Himalayan syntaxis. *Geosphere, 15*, 856–881.

Haproff, P.J., Odlum, M.L., Zuza, A.V., Yin, A., & Stockli, D.F. (2020). Structural and thermochronologic constraints on the Cenozoic tectonic development of the northern Indo-Burma Ranges. *Tectonics, 39*, e2020TC006231. https://doi.org/10.1029/2020TC006231

Harrison, T.M., Célérier, J., Aikman, A.B., Hermann, J., & Heizler, M.T. (2009). Diffusion of ^{40}Ar in muscovite. *Geochimica et Cosmochimica Acta, 73*, 1039–1051.

Hawthorne, F.C., Oberti, R., Harlow, G., Maresch, W.V., Martin, R.F., Schumacher, J.C., & Welch, M.D. (2012). Nomenclature of the amphibole supergroup. IMA Report. *American Mineralogist, 97*, 2031–2048.

Holdaway, M.J. (2000). Application of new experimental and garnet Margules data to the garnet-biotite geothermometer. *American Mineralogist, 85*, 881–892.

Hu, X., Garzanti, E., Wang, J., Huang, W., & Webb, A.A.G. (2016). The timing of India–Asia collision onset – facts, theories, controversies. *Earth-Science Reviews, 160*, 264–299.

Hynes, A., & Forest, R.C. (1988). Empirical garnet-muscovite geothermometry in low-grade metapelites, Selwyn Range (Canadian Rockies). *Journal Metamorphic Geology, 6*, 297–309.

382 Jarosewich, E., Nelen, J.A., & Norberg, J.A. (1980). Reference samples for electron
383 microprobe analysis. *Geostandard Newsletter, 4*, 43–47.
384 Käßner, A., Ratschbacher, L., Jonckheere, R., Enkelmann, E., Khan, J., Sonntag, B.-L.,
385 Gloaguen, R., Gadoev, M., & Oimahmadov, I. (2016). Cenozoic intracontinental
386 deformation and exhumation at the northwestern tip of the India-Asia
387 collision–southwestern Tian Shan, Tajikistan, and Kyrgyzstan. *Tectonics, 35*, 2171–2194.
388 Kooijman, E., Mezger, K., and Berndt, J. (2010). Constraints on the U–Pb systematics of
389 metamorphic rutile from in situ LA ICP-MS analysis. *Earth Planetary Science Letters,*
390 *293*, 321–330.
391 Kornfeld, D., Eckert, S., Appel, E., Ratschbacher, L., Sonntag, B.L., Pfänder, J.A., Ding, L., &
392 Liu, D. (2014). Cenozoic clockwise rotation of the Tengchong block, southeastern
393 Tibetan Plateau: a paleomagnetic and geochronologic study. *Tectonophysics, 628*,
394 105–122.
395 Kretz, R. (1983). Symbols for rock-forming minerals. *American Mineralogist, 68*, 277–279.
396 Kylander-Clark, A.R.C., Hacker, B.R., & Cottle, J.M. (2013). Laser-ablation split-stream ICP
397 petrochronology. *Chemical Geology, 345*, 99–112.
398 Laskowski, A.K., Kapp, P., Vervoort, J.D., & Ding, L. (2016). High-pressure Tethyan
399 Himalaya rocks along the India-Asia suture zone in southern Tibet. *Lithosphere, 8*,
400 574–582.
401 Laskowski, A.K., Kapp, P., Ding, L., Campbell, C., & Liu, X.H. (2017). Tectonic evolution of
402 the Yarlung suture zone, Lopu Range region, southern Tibet. *Tectonics, 36*, 108–
403 136.
404 Li, S., van Hinsbergen, D.J.J., Deng, C., Advokaat, E.L., & Zhu, R. (2018). Paleomagnetic
405 constraints from the Baoshan area on the deformation of the Qiangtang-Sibumasu

406 terrane around the eastern Himalayan syntaxis. *Journal of Geophysical Research,*
407 *Solid Earth, 123*, 977–997.
408 Li, Z., Ding, L., Zaw, T., Wang, H., Cai, F., Yao, W., Xiong, Z., Sein, K., & Yue, Y. (2020).
409 Kinematic evolution of the West Burma block during and after India-Asia collision
410 revealed by paleomagnetism. *Journal of Geodynamics, 134*, 101690.
411 https://doi.org/10.1016/j.jog.2019.101690
412 Linnemann, U., Ouzegane, K., Drareni, A., Hofmann, M., Becker, S., Gärtner, A., & Sagawe A.
413 (2011). Sands of west Gondwana: An archive of secular magmatism and plate
414 interactions—A case study from the Cambro-Ordovician section of the Tassili Ouan
415 Ahaggar (Algerian Sahara) using U-Pb-LA-ICP-MS detrital zircon ages. *Lithos, 123*, 188–
416 203.
417 Liu, C-Z., Chung, S-L., Wu, F-Y., Zhang C., Xu, Y., Wang, J-G., Chen, Y., & Gua, S. (2016).
418 Tethyan suturing in Southeast Asia: Zircon U-Pb and Hf-O isotopic constraints from
419 Myanmar ophiolites. *Geology, 44*, 311–314.
420 Ludwig, K.R. (2000). SQUID 1.00, A User's Manual. *Berkeley Geochronology Center Special*
421 *Publication, 2.*
422 Ludwig, K. (2008). User's Manual for Isoplot4.5. *Berkeley Geochronology Center Special*
423 *Publication, 4*, 1-75.
424 Maurin, T., Masson, F., Rangin, C., Min, U.T., & Collard, P. (2010). First global positioning
425 system results in northern Myanmar: constant and localized slip rate along the
426 Sagaing fault. *Geology, 38*, 591–594.
427 Mitchell, A. (2018). *Geological Belts, Plate Boundaries, and Mineral Deposits in Myanmar.*
428 Amsterdam, Netherlands, Elsevier, 524 p.

429 Morley, C.K., & Arboit, F. (2019). Dating the onset of motion on the Sagaing fault:
430 Evidence from detrital zircon and titanite U-Pb geochronology from the North
431 Minwun Basin, Myanmar. *Geology, 47*, 581–585.
432 Paton, C., Hellstrom, J.C., Paul, B., Woodhead, J.D., & Hergt, J.M. (2011). Iolite: Freeware for
433 the visualisation and processing of mass spectrometer data. *Journal of Analytical*
434 *Atomic Spectrometry, 26*, 2508–2518.
435 Pfänder, J. A., Sperner, B., Ratschbacher, L. Fischer, A., Meyer, M., & Leistner, M. (2014).
436 High-resolution $^{40}Ar/^{39}Ar$ dating using a mechanical sample transfer system combined
437 with a high-temperature cell for step heating experiments and a multi-collector ARGUS
438 noble gas mass spectrometer. *Geochemistry, Geophysics, Geosystems, 15,* 2713–2726.
439 Pownceby, M.-I., Wall, V.-J., & O'Neill, H.S.C. (1987). Fe-Mn partitioning between garnet and
440 ilmenite; experimental calibration and applications. *Contributions to Mineralogy and*
441 *Petrology, 97*, 116–126.
442 Qiu, Z., Wu, F-Y., Yang, S-F., Zhu, M., Sun, J-F., & Yang, P. (2009). Age and genesis of the
443 Myanmar jadeite: constraints from U-Pb ages and Hf isotopes of zircon inclusions.
444 *Chinese Science Bulletin, 54*, 658–668.
445 Ratschbacher, L., Frisch, W., Liu, G., & Chen, C.C. (1994). Distributed deformation in
446 southern and western Tibet during and after the India–Asia collision. *Journal*
447 *Geophysical Research, 99*, 19,917–19,945.
448 Robinson, R.A.J., Brezina, C.A., Parrish, R.R., Horstwood, M.S.A., Nay Win Oo, Bird, M.I.,
449 Myint Thein, Walters, A.S., Oliver, G.J.H., & Khin Zaw (2014). Large rivers and
450 orogens: The evolution of the Yarlung Tsangpo–Irrawaddy system and the eastern
451 Himalayan syntaxis. *Gondwana Research, 26*, 112–121.
452 Rutte, D., Pfänder, J.A., Koleška, M., Jonckheere, R., & Unterricker, S. (2015). Radial fast-
453 neutron fluence gradients during rotating $^{40}Ar/^{39}Ar$ sample irradiation recorded with

454 metallic fluence monitors and geological age standards. *Geochemistry, Geophysics,*
455 *Geosystems, 16*, 336–345.
456 Rutte, D., Ratschbacher, L., Khan, J., Stübner, K., Hacker, B.R., Stearns, M.A., Enkelmann, E.,
457 Jonckheere, R., Pfänder, J.A., Sperner, B., & Tichomirowa, M. (2017) Building the Pamir-
458 Tibet Plateau—Crustal stacking, extensional collapse, and lateral extrusion in the
459 Central Pamir: 2. Timing and rates. *Tectonics, 36*, 385–419.
460 Salvi, D., Mathew, G., Kohn, B., Pande, K., & Borgohain, B. (2019). Thermochronological
461 insights into the morphotectonic evolution of Mishmi hills across the Dibang Valley,
462 NE Himalayan Syntaxis. *Journal of Asian Earth Sciences, 190*, 104158.
463 https://doi.org/10.1016/j.jseaes.2019.104158
464 Shi, G., Cui, W., Cao, S., Jian, N., Jian, P., Liu, D., Miao, L., & Chu, B. (2008). Ion microprobe
465 zircon U-Pb age and geochemistry of the Myanmar jadeitite. *Journal Geological*
466 *Society of London, 165*, 221–234.
467 Spear, F.S. (1993). *Metamorphic Phase Equilibria and Pressure-temperature-time Paths.*
468 Mineralogical Society of America Monographs, 799 pp.
469 Stübner, K., Ratschbacher, L., Weise, C., Chow, J., Hofmann, J., Khan, J., Rutte, D., Sperner, B.,
470 Pfänder, J.A., Hacker, B.R., Dunkl, I., Tichomirowa, M., & Stearns, M.A. (2013). The giant
471 Shakhdara migmatitic gneiss dome, Pamir, India-Asia collision zone: 2. Timing of dome
472 formation. *Tectonics, 32*, 1404–1431,
473 Thomas, J. B., Watson, E. B., Spear, F. S., Shemella, P. T., Nayak, S. K., & Lanzirotti, A. (2010).
474 TitaniQ under pressure: The effect of pressure and temperature on the solubility of Ti
475 in quartz. *Contributions to Mineralogy and Petrology, 160*, 743–759.
476 Van Hinsbergen, D.J.J., Lippert, P.C., Dupont-Nivet, G., McQuarrie, N., Doubrovine, P.V.,
477 Spakman, W., & Torsvik, T.H. (2012). Greater India basin hypothesis and a two-

478 stage Cenozoic collision between India and Asia. *Proceedings of the National*
479 *Academy of Science, 109*, 7659–7664.
480 Wauschkuhn, B., Jonckheere, R., & Ratschbacher, L. (2015). The KTB apatite fission-track
481 profiles: Building on a firm foundation? *Geochimica et Cosmochimica Acta, 167*, 27–62.
482 Westerweel, J., Roperch, P., Licht, A., Dupont-Nivet, G., Win, Z., Poblete, F., Ruffet, G., Swe,
483 H.H., Thi, M.K., & Aung, D.W. (2019). Burma terrane part of the Trans-Tethyan arc
484 during collision with India according to paleomagnetic data. *Nature Geoscience, 12*,
485 863–868.
486 Wang, E., & Burchfiel, B.C. (1997). Interpretation of Cenozoic tectonics in the right-
487 lateral accommodation zone between the Aialo Shan shear zone and the Eastern
488 Himalayan Syntaxis. *International Geological Review, 39*, 191–219.
489 Warren, C.J., Hanke, F., & Kelley, S.P. (2012). When can muscovite $^{40}Ar/^{39}Ar$ dating
490 constrain the timing of metamorphic exhumation? *Chemical Geology, 291*, 79–86.
491 Wiedenbeck, M., Alle, P., Corfu, F., Griffin, W.L., Meier, M., Oberli, F., Von Quadt, A.,
492 Roddick, J.C., & Spiegel, W. (1995). Three natural zircon standards for U-Th-Pb, Lu-Hf,
493 trace element and REE analyses. *Geostandards Newsletter, 19*, 1-23.
494 Williams, I.S. (1998). U-Th-Pb geochronology by ion microprobe. *Reviews in Economic*
495 *Geology, 7*, 1-35.
496 Yang, J.S., Xu, Z.Q., Duan, X.D., Xiong, F.H., Liu, Z., Cai, Z.H., & Li, H.Q. (2012). Discovery of a
497 Jurassic SSZ ophiolite in the Myitkyina region of Myanmar. *Acta Petrologica Sinica,*
498 *28*, 1710–1730.
499 Zhang, P.Z., Shen, Z., Wang, M., Gan, W., Bürgmann, R., Molnar, P., Wang, Q., Niu, Z., Sun, J.,
500 Wu, J., & Hanrong, S. (2004). Continuous deformation of the Tibetan Plateau from
501 global positioning system data. *Geology, 32*, 809–812.

Zhang, J., Xiao, W., Windley, B.F., Wakabayashi, J., Cai, F., Seing, K., Wu, H., & Naing, S. (2018). Multiple alternating forearc- and backarc-ward migration of magmatism in the Indo-Myanmar Orogenic Belt since the Jurassic: Documentation of the orogenic architecture of eastern Neotethys in SE Asia. *Earth-Science Reviews, 185*, 704–731.

Zubovich, A.V., Wang, X Q., Scherba, Y.G., Schelochkov, G.G., Reilinger, R., Reigber, C., et al. (2010). GPS velocity field of the Tien Shan and surrounding regions. *Tectonics*, *29*, TC6014. https://doi.org/10.1029/2010TC002772